51st AIAA Aerospace Sciences Meeting including the New Horizons Forum and Aerospace Exposition
07 - 10 January 2013, Grapevine (Dallas/Ft. Worth Region), Texas

AIAA 2013-0490

Performance of Co-Flow Jet Airfoil with Variation of Mach Number

A. Lefebvre[*], B. Dano[†], M. D. Fronzo[‡], W. B. Bartow[§], G.-C. Zha[¶]
Dept. of Mechanical and Aerospace Engineering
University of Miami
Coral Gables, Florida 33124
E-mail: gzha@miami.edu

Abstract

This paper conducts numerical investigations for a 15% thickness Co-Flow Jet (CFJ) airfoil performance enhancement, which includes the variation of lift, drag, and energy expenditure at Mach number 0.03, 0.3, and 0.4 with jet momentum coefficient $C_\mu = 0.08$. The angle of attack(AoA) varies from 0° to 30°. Two-dimensional simulation is conducted using a Reynolds-averaged Navier-Stokes (RANS) solver. A 5th order WENO scheme for the inviscid flux and a 4th order central differencing for the viscous terms are used to resolve the the Navier-Stokes equations. Turbulence is simulated with the one equation Spalart-Allmaras model.

The study shows that at constant C_μ, the maximum lift coefficient is increased with the increasing Mach number due to the compressibility effect. However, at M=0.4, the airfoil stalls with slightly lower AoA due to the appearance of strong λ shock wave that interrupts the jet and trigger boundary layer separation. The drag coefficients vary less with the Mach number, but is substantially increased at Mach 0.4 when the AoA is high due to shock wave-boundary layer interaction and wave drag.

The power coefficient is decreased when the Mach number is increased from 0.03 to 0.3. This is again due to the compressibility effect that generates stronger low pressure suction effect at airfoil leading edge, which makes the CFJ pumping easier and require less power. For the same reason of shock appearance at M=0.4 when the AoA is high, the power coefficient is significantly increased due to large entropy increase. Overall, the numerical simulation indicates that the CFJ airfoil is very effective to enhance lift, reduce drag, and increase stall margin with high Mach number up to 0.4 at low energy expenditure.

Nomenclature

AoA	Angle of attack
CFJ	Co-flow jet
P	Power requested from the pump
P_c	Power coefficient
C_L	Lift coefficient
C_D	Drag coefficient
R_e	Reynolds number
M	Mach number
c_p	Specific heat of the air by keeping constant pressure
γ	Air specific heats ratio
S	Planform area of the wing
ρ_∞	Density
V_∞	Velocity
T_t	Total temperature
P_t	Total pressure
H_t	Total specific enthalpy

[*] Ph.D. Candidate
[†] Ph.D., Adjunct Faculty
[‡] Visiting Graduate Student
[§] Master Student
[¶] Associate Professor, AIAA Associate Fellow

$\dot{m}$	Mass flow across the pump
$_\infty$	Subscript, stands for free stream
$_j$	Subscript, stands for jet

1 Introduction

An active flow control (FC) method is to enhance airfoil performance by energizing the flow with minimal or no structural moving parts. When a high lift airfoil flow control technique is developed, three primary issues need to be considered: 1) effectiveness, 2) energy efficiency, and 3) ease of implementation. First, the FC method should provide a substantial improvement in aerodynamic performance, which may include lift enhancement, drag reduction, and stall margin increase. Second, the FC method should not require significant energy expenditure. Otherwise, the penalty may outweigh the benefit for the whole system. Third, the FC technique should not be too difficult to implement. Various FC approaches are briefly summarized below.

The circulation control airfoil [1–3] relies on the Coanda effect, which creates a locally favorable pressure gradient on a curved surface to attach the flow. Such a favorable pressure gradient exists at the airfoil LE due to suction and in the vicinity of a blunt TE due to the low base pressure. Hence, a blunt TE is usually required to render CC effective. However, this will create large drag at cruise conditions. To overcome the dependence on a blunt TE for circulation control airfoil, a movable flap at the airfoil TE has been suggested by Englar [4]. Unfortunately, such moving parts impose a weight penalty. At large angles of attack (AoA), the flow cannot overcome the large adverse pressure gradient. As a result, a favorable pressure gradient near the TE cannot be achieved and, hence, the Coanda effect is difficult to realize. If only TE blowing is used, a circulation-controlled airfoil will stall at a smaller AoA than a non-controlled airfoil [5]. To maintain sufficient stall margin, LE blowing also needs to be added [5].

A considerable penalty of CC is the dumped blowing jet mass flow, which is imposed on the propulsion system. This is because the supply air for control is usually obtained from the engine compressor bleed. The resultant decrease in thrust is directly proportional to the mass flow rate of the engine bleed; i.e., an engine will incur a 1% thrust decrease for a 1% bleed flow and will result in a 1-3% fuel consumption increase depending on whether the bleed is from the compressor front or back stage. Furthermore, for a CC airfoil, the drag measured in the wind tunnel is not the actual drag that will occur on the aircraft. This is because, in the wind tunnel, the penalty to draw the mass flow from the freestream as the supply for the jet injection is not included in the drag measurement. The actual drag, also called the "equivalent" drag, needs to include this penalty [6, 7]. The penalty to draw mass flow from the freestream includes ram drag and captured area drag. The equivalent drag of a CC airfoil is thus significantly larger than the drag measured in the wind tunnel [6].

To reduce the penalty associated with CC due to the dumped jet mass flow and the equivalent drag, a pulsed jet can be used [7] and is able to significantly reduce the jet mass flow rate. Recently, other promising methods using zero-net mass flux (ZNMF) synthetic jets [8, 9] and dielectric-barrier discharge plasma actuators [10, 11] are being developed. These approaches avoid dumping the jet mass flow. However, at present, both ZNMF and plasma actuators are generally lacking in terms of sufficient actuator authority for high speed flows.

Recently, a promising ZNMF co-flow jet flow control airfoil based on fluidic actuators (hereafter co-flow jet airfoil or CFJ airfoil) has been developed by Zha et al. [6, 12–18]. The CFJ airfoil achieves three effects simultaneously in a radical manner: lift augmentation, stall margin increase, and drag reduction. The energy expenditure of the CFJ airfoil is low [6, 17], and the CFJ airfoil concept is straightforward to implement.

1.1 The ZNMF CFJ Airfoil

In the CFJ airfoil concept [6, 12–18], an injection slot near leading edge and a suction slot near trailing edge on the airfoil suction surface are created as sketched in Fig. 1. A small amount of mass flow is withdrawn into the airfoil near the trailing edge(TE), pressurized and energized by a pumping system inside the airfoil, and then injected near the leading edge(LE) in the direction tangent to the main flow. The whole process does not add any mass flow to the system and hence is a ZNMF flow control.

The CFJ airfoil flow process provides a unique low energy expenditure ZNMF flow control, which has the injection near the suction peak of the airfoil where the lowest main flow pressure is located, and jet suction at the near trailing edge where the highest main flow pressure is located. In other words, the required pumping work of CFJ airfoil would be lower than those of the flow control methods injecting near trailing edge such as a CC airfoil. Furthermore,

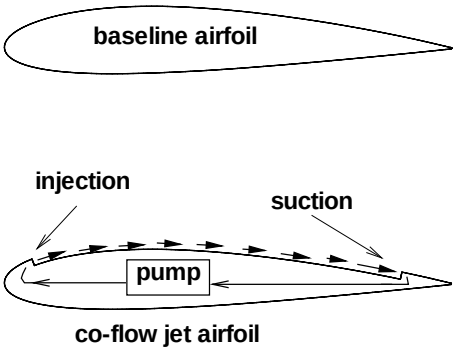

Figure 1: Baseline airfoil and CFJ Airfoil.

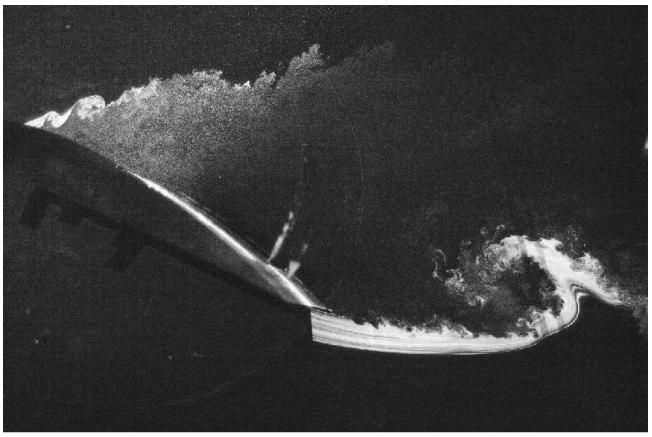

Figure 2: Massive flow separation of baseline NACA 6415 airfoil at AoA=25°.

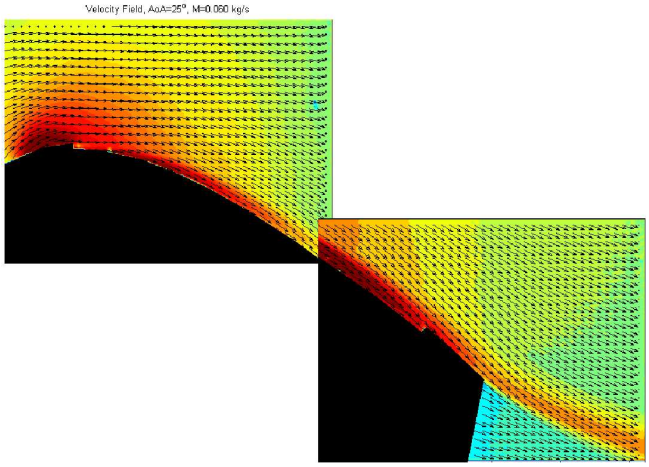

Figure 3: Attached flow of CFJ NACA 6415 airfoil at AoA=25° measured by PIV in experiment.

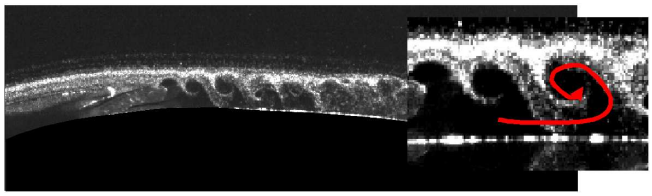

Figure 4: Coherent vortex structures in the region of CFJ airfoil injection, AoA=5°, $C_\mu = 0.02$.

a flow control method using injection only will have to do more work to overcome the ram and captured area drag, which do not exist for CFJ airfoil due to the ZNMF [6]. As pointed out in [6], the injection and suction of CFJ airfoil are efficiently integrated and they both enhance boundary layer momentum and airfoil circulation.

The fundamental mechanism of CFJ airfoil is that the turbulent mixing between the jet and main flow makes a lateral transport of energy between the jet, boundary layer, and main flow to energize the wall boundary layer. The large vortex structures and adverse pressure gradient are all beneficial to enhance mixing. The mixing allows the flow to overcome a large adverse pressure gradient and remain attached at a very high angle of attack. Hence, the stall margin is significantly increased. At the same time, the energized boundary layer drastically increases the circulation, augments lift, and reduces the total drag or generates thrust (net negative drag). The portion of CFJ energy used to overcome the increased local drag due to higher jet speed is small since the mixing occurs immediately when the jet penetrates into the boundary layer under an adverse pressure gradient. Unlike a jet in cross flow (JICF) which enhances mixing between the jet and main flow but retards the main flow due to the cross flow blockage created by the jet, the co-flow jet mixing only enhances the streamwise flow momentum since the jet is tangential to the main flow. The momentum retardation due to JICF will result in a significant entropy and drag increase.

The thrust generation or drag reduction by a CFJ airfoil can be explained by two mechanisms [6, 12–14]: First, due to the very high circulation, the LE suction is so strong that the low pressure at the LE results in a thrust when the AoA is below a certain value. The slightly increased local surface friction due to higher jet velocity is offset by

this LE super-suction, or pressure drag reduction, which is the same mechanism that bird wings generate thrust at down stroke flapping at high AoA. Second, the energized main flow fills the wake and reduce velocity deficit. From control volume analysis, it is known that a shallower wake velocity deficit means a smaller drag. When the wake velocity deficit is reversed, the airfoil will generate a thrust, which occurs for CFJ airfoil as demonstrated in both experiments and numerical simulation [6,12–17]. CFJ airfoil appears to be the only flow control method that generate both significant lift and thrust at the same time. It is because a CFJ airfoil benefits greatly from the tangential jet injection momentum even though the jet suction will offset the benefit. Fig. 2 shows a massive flow separation of baseline NACA 6415 airfoil at AoA of 25° in our wind tunnel testing [16]. Fig. 3 is the PIV measured velocity field with CFJ at the same AoA, which demonstrates that the flow is attached with a higher speed within the wake than in the freestream, a reversed wake deficit or jet. In this case, a thrust is generated. The flow is attached at a momentum coefficient $C_\mu = 0.06$ for this case.

Fig. 5 compares the lift coefficient of CFJ airfoils with baseline airfoil at the momentum coefficient $C_\mu = 0.08$. The CFJ airfoils have different slot blockages to generate discrete holes and hence different jet velocity while keeping the same mass flow rate. For example, the open slot (black solid circles) has zero blockage. The symbol OF stands for the obstruction factor (blockage), which is the percentage of the slot area blocked. OF of 3/4 means that 75% of the injection slot area is blocked and it results in many small discrete holes for the CFJ injection. Fig. 5 shows that the open slot CFJ airfoil increases the maximum lift coefficient by about 50%, whereas the discrete CFJ airfoil with OF of 2/3 increases the lift by about 100%. When the momentum coefficient is increased, the maximum lift coefficient is further augmented.

A unique feature of CFJ airfoil is to generates a large thrust while increasing the lift due to efficient energizing streamwise momentum of the flow. Fig. 6 shows all the airfoils generate thrust (negative drag) with the maximum amount produced by a CFJ airfoil using discrete jets with obstruction factor of 3/4. The minimum drag is reduced by 4000% to an enormous thrust coefficient of about 0.8. By comparing with the open slot CFJ airfoil, the discrete CFJ (DCFJ) airfoil needs half of the mass flow rate to achieve the same lift augment and drag reduction [17]. However, the power consumed by the DCFJ is significantly higher than the open slot CFJ airfoil since the smaller holes create more blockage loss for the jets. Nonetheless, the extraordinary high lift and high thrust generated by the DCFJ deserve the extra energy cost [17]. In nature, the only system that generates both lift and thrust at the same time is bird flapping wings. In the man made fixed wing systems, CFJ airfoil seems to be the only one that can achieve such effect.

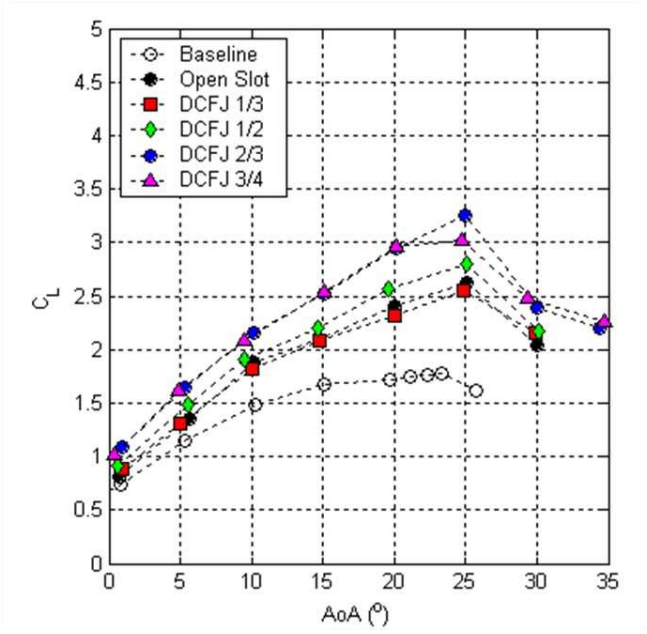

Figure 5: Comparison of lift coefficient of CFJ airfoils with different obstruction factors, $C^*_\mu = 0.08$.

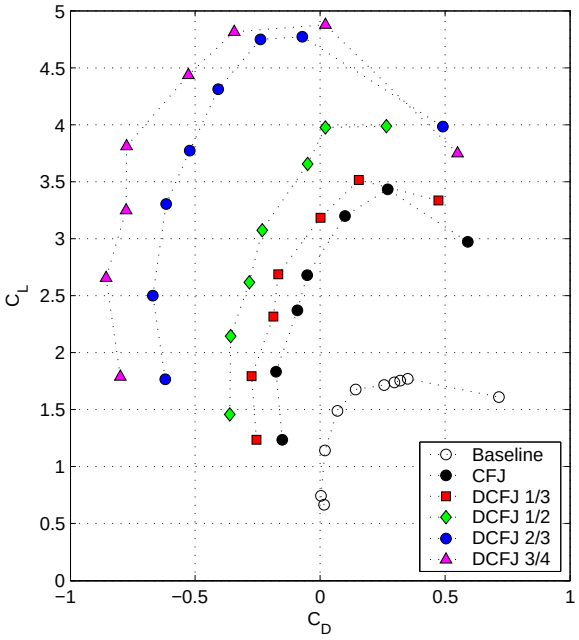

Figure 6: Comparison of the drag polars of discrete CFJ airfoils with different obstruction factors, $C^*_\mu = 0.25$.

The CFJ airfoil shows great potential to enhance the airfoil performance and the low energy expenditure of the CFJ airfoil makes it very attractive. Dano et al. [17] investigate the energy expenditure of the CFJ airfoil at Mach number of 0.03, which indicates that the CFJ airfoil gain tremendous performance enhancement at high angle of attack at low energy expenditure. So far, most of the airfoil active flow control techniques are used for low Mach number without shock waves appearing.

1.2 Objective

The objective of this paper is to study the CFJ airfoil energy expenditure and performance enhancement with the variation of Mach number from 0.03 to 0.4. A useful flow control method for helicopter blades to mitigate dynamic stall would be desirable to work up to Mach number range of 0.4 to 0.5. The challenge at this Mach number range is that a strong transonic shock may appear at high AoA, which may significantly reduce the effectiveness of a flow control technique. Little airfoil flow control study has been done at this Mach number range. This paper is to make the first effort to study CFJ airfoil performance at the high freestream Mach number as a potential candidate for pitching airfoil flow control.

2 CFJ parameters

2.1 Jet Momentum Coefficient

The jet momentum coefficient C_μ is a parameter used to quantify the jet intensity. It is defined as :

$$C_\mu = \frac{\dot{m}V_j}{\frac{1}{2}\rho_\infty {V_\infty}^2 S} \tag{1}$$

where $\dot{m}$ is the injection mass flow, V_j represents the injection jet velocity, ρ_∞ and V_∞ denote the free stream density and velocity, respectively, and S is the planform area.

2.2 Power Coefficient

The CFJ can be conceptually implemented by mounting a pumping system inside the wing that withdraws air from the suction cavity and blows it into the injection cavity. The power consumption can be determined by the jet mass flow and total enthalpy change as the following :

$$P = \dot{m}(H_{t1} - H_{t2}) \tag{2}$$

where H_{t1} and H_{t2} are the total enthalpy in the injection cavity and suction cavity respectively, P is the Power required by the pump and $\dot{m}$ the injection mass flow rate. Introducing the pump efficiency η and total pressure ratio of the pump $\Gamma = \frac{P_{t1}}{P_{t2}}$, the power consumption can be expressed as :

$$P = \frac{\dot{m}C_pT_{t2}}{\eta}(\Gamma^{\frac{\gamma-1}{\gamma}} - 1) \tag{3}$$

The pumping efficiency of 80% is used in this study for both the experiment and CFD to represent a conservative estimate of a typical pumping system. The power consumption can be expressed as a power coefficient below:

$$P_c = \frac{P}{\frac{1}{2}\rho_\infty V_\infty^3 S} \tag{4}$$

2.3 Jet Effect on Lift and Drag

By using a control volume analysis, Zha et al. derived an expression for the force effect of the injection and suction jets on the CFJ airfoil [19]. Based on the Newton's third law, the momentum and pressure at the injection and suction slots produce a reactionary force, which must be taken into account in the drag and lift calculations. The expressions for these reactionary forces are given as:

$$F_{x_{cfj}} = (\dot{m}_j V_{j1} + p_{j1} A_{j1}) * cos(\theta_1 - \alpha) - (\dot{m}_j V_{j2} + p_{j2} A_{j2}) * cos(\theta_2 + \alpha) \tag{5}$$

$$F_{y_{cfj}} = (\dot{m}_j V_{j1} + p_{j1} A_{j1}) * sin(\theta_1 - \alpha) - (\dot{m}_j V_{j2} + p_{j2} A_{j2}) * sin(\theta_2 + \alpha) \tag{6}$$

Where the subscripts 1 and 2 stand for the injection and suction respectively, and θ_1 and θ_2 are the angles between the injection and suction slot surface and a line normal to the airfoil chord [19]. The total lift and drag on the airfoil can then be expressed as:

$$D = R'_x - F_{x_{cfj}} \tag{7}$$

$$L = R'_y - F_{y_{cfj}} \tag{8}$$

Where R'_x and R'_y are the surface integral of pressure and shear stress in x (drag) and y (lift) direction. For the CFD simulation, the total lift and drag are calculated using Eqs.(7) and (8).

3 CFD Simulation

3.1 Modeling parameters

The FASIP (Flow-Acoustics-Structure Interaction Package) CFD code is used to conduct the numerical simulation. The 2D Reynolds averaged Navier-Stokes (RANS) equations with one-equation Spalart-Allmaras [20] turbulence model is used. A 5th order WENO scheme for the inviscid flux [21–27] and a 4th order central differencing for the viscous terms [21,26] are employed to discretize the Navier-Stokes equations. The low diffusion E-CUSP scheme used as the approximate Riemann solver suggested by Zha et al [22] is utilized with the WENO scheme to evaluate the inviscid fluxes. Implicit time marching method using Gauss-Seidel line relaxation is used to achieve fast convergence rate [28]. Parallel computing is implemented to save wall clock simulation time [29]. The RANS solver is validated for CFJ airfoil simulation [15].

3.2 Boundary Conditions

The wall treatment suggested in [25] to achieve the flux conservation by shifting half interval of the mesh on the wall is employed. The 3rd order accuracy no slip condition is enforced on the solid surface as described in [25]. Total pressure, total temperature and flow angle are specified as the inlet boundary conditions for the upstream portion of the farfield boundary and inside the injection cavity. Constant static pressure is used downstream at the farfield boundary and in the suction cavity.

To achieve zero net mass flux with the CFJ flow control, the mass flow that exits the injection slot must equal the mass flow entering the suction slot. Additionally, the jet strength must be controlled in order to reach the prescribed C_μ. This is achieved by a subroutine which calculates the difference between actual C_μ and the C_μ prescribed by a user and adjusts the total pressure inside the injection cavity using a linear interpolation law. Total temperature is assumed constant during this process. If actual C_μ falls within 1% of the prescribed value, no modification is made to the total pressure. At the suction cavity, the subroutine compares the injection and suction mass flow and adjusts the static pressure at the suction cavity until the injection and suction mass flow match. The process is iterated throughout the simulation until the specified momentum coefficient is reached.

4 Wind Tunnel Experiments [16–18]

The airfoil used for baseline comparison is a NACA 6415 with the chord length of 12" and span of 24". The CFJ airfoil was a NACA 6415 with the injection and suction located at 7.5% and 88.5% of the chord, respectively. The injection and suction slot heights were 0.65% (2.0 mm) and 1.42% (4.0 mm) of the chord. In the experiment, the CFJ is provided by a separated high pressure source for the injection and a low pressure vacuum sink for the suction. Pressurized air is injected in a spanwise long cavity near the LE, and then exits through a spanwise long rectangular

slot. A Duocel high density aluminum foam (HDF) was placed between the inlet and the injection slot to equilibrate the pressure and ensure a uniform exit velocity. Similarly, a spanwise long cavity placed near the TE is used to let the air settle down before being sucked through three suction ports.

All airflow and aerodynamic variables were acquired at the University of Miami 24"x 24" wind tunnel facilities. The injection and suction flow conditions were independently controlled. A compressor supplies the injection flow line and the flow rate controlled using a $Koso^{TM}$ Hammel Dahl computer controlled valve. A vacuum pump generates the necessary low pressure for suction and is controlled with a manual needle valve. Both mass flow rates in the injection and suction lines are measured using $Oripac^{TM}$ orifice mass flowmeters equipped with high precision MKS pressure transducers. Total pressure and temperature probes were places inside the injection and suction cavities. The aerodynamics variables are measured using an $AMTI^{TM}$ 6 component transducer. All wind tunnel freestream, CFJ airflow and aerodynamic variables were recorded using a state-of-the-art $Labview^{TM}$ data acquisition system. All the data (e.g., wind tunnel speed, aerodynamic forces, blowing and suction mass flow rates) were acquired at a rate of approximately 50 samples per seconds. For the testing case at Mach number 0.03, leading edge trip was used to achieve full turbulent boundary layer to be consistent with the CFD analysis.

5 Mesh

The computation mesh is constructed using the O-mesh topology in order to achieve high quality mesh around the airfoil. A total of 451 points are placed around airfoil, 301 points on suction surface and 151 points on the pressure surface, 101 points normal to the airfoil with an additional 31 points across the jet. Total mesh size is 55,500 cells, partitioned into 12 blocks for the parallel computation. The farfield boundary is located 30 chord away from the airfoil. To resolve the turbulent boundary layer, the first grid point is placed at $y^+ \approx 1$. Block definition can be found in Table 1 and the mesh topology is shown in Fig. 7.

Block	ξ-Direction	η-Direction	Cell number
1-9	51	101	5000
10	101	31	3000
11	151	31	4500
12	101	31	3000
Total mesh size			55500

Table 1: Block dimension for CFJ6415 airfoil

A mesh refinement was performed at M=0.3 by increasing the mesh size by 50% in every direction. The results are in excellent agreement with the baseline mesh.

6 Results

The CFJ airfoil modified from NACA6415 airfoil, which is experimentally studied by Dano et al in [16–18] with Mach number of 0.03, is first simulated to validate the CFD solver. The Mach number is then increased to 0.3 and 0.4. The jet momentum coefficient is $C_\mu = 0.08$ for all the Mach numbers. The angle of attack varies from 0° to 30° at an increment of 5°.The Reynolds numbers based on freestream velocity and chord length are listed in Table 2.

$Mach$	$V_\infty(m/s)$	$R_e.10^5$
0.03	10.297	2.078
0.3	102.968	20.779
0.4	137.290	33.386

Table 2: Reynolds number function of free stream velocity and Mach number

6.1 CFD Validation at M=0.03

Fig. 8 shows the computed lift, drag and power coefficient compared with the experiment for the baseline airfoil and the CFJ airfoil at $M = 0.03$. For the lift, good agreement is obtained up to AoA of 20° when the flow is mostly attached. The computed drag is significantly under-predicted when the AoA is greater than 10°. However, the predicted power coefficient agrees well with the experiment. For the power coefficient plot on the bottom of Fig. 8, The left vertical axis represents the dimensionless power coefficient while the right vertical axis is the required pumping power in watt for a pumping efficiency of 80%. The reason why the predicted power consumption agrees well with the experiment may be that the total pressure and total temperature are integrated parameters using mass average, which is easier to predict accurately than the drag that is determined by skin friction. It is observed that the power coefficient decreases with the increase of AoA up to 15° and rises at higher AoA. The reason appears to be that when the AoA is increased and the flow is not separated, the airfoil leading edge suction effect becomes stronger with lower static pressure in the region of the injection jet, and hence less power is needed to generate the jet with the same momentum coefficient. However, when the AoA is beyond the separation value, the boundary layer separation creates very large energy loss and the suction power is significantly increased.

6.2 Performance with Increased Mach Number

Fig. 9 shows the computed lift, drag and power coefficient comparison at different Mach numbers. The baseline airfoil Lift and drag show little dependency on the free stream velocity, and is hence plot at M=0.3 only. At constant C_μ, the lift coefficient is increased with the increased Mach number. The maximum C_L reaches 2.8 at $M = 0.4$. This is due to the compressibility effect at higher Mach number with a stronger suction effect at leading edge. However, at M=0.4, the airfoil stalls earlier due to the appearance of strong shock wave on the suction surface as to be shown later. The drag coefficient vary less with the Mach number, but is also significantly increased at Mach 0.4 when the AoA is greater than 15° due to the shock wave-boundary layer interaction and wave drag. The power coefficient decreases when the Mach number is increased from 0.03 to 0.3. This is due to the compressibility effect that generates lower pressure at the suction side leading edge, which reduces the pumping energy necessary to create the jet. At M=0.4, the power coefficient at AoA=0° is about the same as at Mach 0.3 and is significantly lower than at Mach 0.03. However, with the AoA increased up to 15°, the power coefficient at Mach 0.4 remains fairly flat instead of decreasing as at Mach 0.3. The reason is that the flow reaches sonic or supersonic with the increased AoA and the energy loss is increased, in particular when shock waves appear as shown later. When the AoA is greater than 15°, the strong shock wave boundary layer interaction generates very large entropy increase and makes the power required increase significantly. Fig. 9 also shows the refined mesh results for C_L, C_D and P_c at Mach 0.3. They are virtually identical to the baseline mesh results and indicate that the present CFD simulations are converged based on mesh size.

Fig. 10 shows the pressure coefficient on the baseline and CFJ airfoil at various AoA with free stream Mach number of 0.3. The injection and suction spikes appear because the pressure coefficient is measured on a discontinuous surface. The CFJ greatly lowers the pressure on the suction surface and increases the lift. The pressure has a significantly higher peak than the baseline airfoil, increasing the lift. Due to the peak location at the leading edge of the profile, the drag is reduced. This proves that CFJ airfoil have better lift due to their overall lower pressure on the suction surface, but as importantly, CFJ airfoil have a pressure repartition on their surface that reduces the pressure drag.

The power coefficient is determined by the total pressure ratio between the injection and suction as indicated by Eq. 4. Fig. 11 shows the total pressure variation with AoA at injection and suction location. It indicates that the injection total pressure decreases monotonically with AoA. This is because when AoA is increased, the static pressure at the injection region is decreased. In order to keep the same C_μ, the injection total pressure must be decreased to achieve about the same injection jet mass flow rate. However, the suction total pressure decreases much more after AoA=15° due to deteriorated kinetic energy of the boundary layer caused by flow separation. This makes the required power decrease when the AoA varies from 0° to 15° as shown in Fig. 11, and the power is increased when AoA is higher than 15° due to the higher loss of the suction total pressure.

Fig. 12, 13 and 14 show the Mach number contours with streamlines for the CFJ airfoil at $AoA = 0°$, 10° and 20° for $M = 0.03$, 0.3, and 0.4 with $C_\mu = 0.08$. The CFJ enhances the suction surface acceleration very effectively at low AoA, which increases the lift. At $AoA = 20°$, there is mild separation for the Mach 0.03 and 0.3, but a significant separation occurs for Mach 0.4 due to the shock wave boundary layer interaction occurring at the injection jet region to be shown later in Fig. 17.

Fig. 15, 16 and 17 show the Mach number contours at the injection jet region for different Mach numbers. For M=0.03, all the flow field with CFJ is subsonic as expected. When Mach number is increased to 0.3, the jet exit

velocity is transonic. At $AoA = 20°$, a supersonic region appears in the leading edge region with the maximum Mach number about 1.4. Free stream Mach number of 0.3 is still very favorable for lift increase and drag reduction at low power expenditure since the shocks are not too strong and are still mostly in the near isentropic region.

When the Mach number reaches 0.4, the flow field structure is very different, characterized by the supersonic flow and shock waves as shown in Fig. 17. At $AoA = 0°$, the injection jet already reaches Mach 1.5. At $AoA = 10°$, the injection jet speed is further increased due to the decreased main flow static pressure at injection region, and a weak shock forms downstream of the injection slot. However the jet remains uninterrupted. At $AoA = 20°$, the injection jet Mach number reaches 2.2. A strong λ shock appears in the injection exit region. The rear leg of the λ shock has greater strength, interrupts the jet, and causes significant flow separation, which is reflected by the higher drag and power coefficient and reduced stall AoA as shown in Fig. 9.

7 Conclusions

The performance of a co-flow Jet airfoil with variation of Mach number is investigated. The study shows that at constant C_μ, the maximum lift coefficient is increased with the increasing Mach number due to the compressibility effect. However, at M=0.4, the airfoil stalls with slightly lower AoA due to the appearance of strong λ shock wave that interrupts the jet and trigger boundary layer separation. The drag coefficients vary less with the Mach number, but is substantially increased at Mach 0.4 when the AoA is high due to shock wave-boundary layer interaction and wave drag.

The power coefficient is decreased when the Mach number is increased from 0.03 to 0.3. This is again due to the compressibility effect that generates stronger low pressure suction effect at airfoil leading edge, which makes the CFJ pumping easier and require less power. For the same reason of shock appearance at M=0.4 when the AoA is high, the power coefficient is significantly increased due to large entropy increase. Overall, the numerical simulation indicates that the CFJ airfoil is very effective to enhance lift, reduce drag, and increase stall margin with high Mach number up to 0.4 at low energy expenditure.

References

[1] R. Englar and R. M. Williams, "Test Techniques for High Lift, Two Dimensional Airfoils with Boundary Layer and Circulation Control for Application to Rotary Wing Aircraft," *Canadian Aeronautics and Space Journal*, vol. 19, pp. 93–108, 1973.

[2] R. J. Englar, "Circulation Control for High Lift and Drag Generation on STOL Aircraft," *Journal of Aircraft*, vol. 12, pp. 457–463, 1975.

[3] R. J. Englar, L. A. Trobaugh, and R. Hemmersly, "STOL Potential of the Circulation Control Wing for High-Performance Aircraft," *Journal of Aircraft*, vol. 14, pp. 175–181, 1978.

[4] R. J. Englar, "Circulation Control Pneumatic Aerodynamics: Blown Force and Moment Augmentation and Modifications; Past, Present and Future." AIAA 2000-2541, June 2000.

[5] Y. Liu, L. N. Sankar, R. J. Englar, K. K. Ahuja, and R. Gaeta, "Computational Evaluation of the Steady and Pulsed Jet Effects on the Performance of a Circulation Control Wing Section." AIAA Paper 2004-0056, 42nd AIAA Aerospace Sciences Meeting and Exhibit, Reno, Nevada 5 - 8 Jan 2004.

[6] G.-C. Zha, W. Gao, and C. Paxton, "Jet Effects on Co-Flow Jet Airfoil Performance," *AIAA Journal, No. 6,*, vol. 45, pp. 1222–1231, 2007.

[7] G. S. Jones, "Pneumatic Flap Performance for a 2D Circulation Control Airfoil, Stedy & Pulsed." *Applications of Circulation Control Technologies*, Chapter 7, p. 191-244, Vol. 214, Progress in Astronautics and Aeronautics, AIAA Book Series, Editors: Joslin, R. D. and Jones, G. S., 2006.

[8] A. Glezer and M. Amitay, "Synthetic Jets," *Annual Review of Fluid Mechanics*, vol. 24, 2002.

[9] R. Holman, Y. Utturkar, R. Mittal, and L. Cattafesta, "Formation Criterion for Synthetic Jets," *AIAA Journal*, vol. 43, No. 10, pp. 2110–2116, 2005.

[10] T. C. Corke and M. L. Post, " Overview of Plasma Flow Control: Concepts, Optimization, and Applications." AIAA Paper 2005-0563, Jan. 2005.

[11] C. Enloe, T. E. McLaughlin, G. I. Font, and J. W. Baughn, " Frequency Effects on the Efficiency of Aerodynamic Plasma Actuator ." AIAA Paper 2006-0166, Jan. 2006.

[12] G.-C. Zha and D. C. Paxton, "A Novel Flow Control Method for Airfoil Performance Enhancement Using Co-Flow Jet." *Applications of Circulation Control Technologies*, Chapter 10, p. 293-314, Vol. 214, Progress in Astronautics and Aeronautics, AIAA Book Series, Editors: Joslin, R. D. and Jones, G.S., 2006.

[13] G.-C. Zha, C. Paxton, A. Conley, A. Wells, and B. Carroll, "Effect of Injection Slot Size on High Performance Co-Flow Jet Airfoil," *AIAA Journal of Aircraft*, vol. 43, 2006.

[14] G.-C. Zha, B. Carroll, C. Paxton, A. Conley, and A. Wells, "High Performance Airfoil with Co-Flow Jet Flow Control," *AIAA Journal*, vol. 45, 2007.

[15] Wang, B.-Y. and Haddoukessouni, B. and Levy, J. and Zha, G.-C., "Numerical Investigations of Injection Slot Size Effect on the Performance of Co-Flow Jet Airfoil," *Journal of Aircraft*, vol. Vol. 45, No. 6,, pp. pp.2084–2091, 2008.

[16] B. P. E. Dano, D. Kirk, and G.-C. Zha, "Experimental Investigation of Jet Mixing Mechanism of Co- Flow Jet Airfoil." AIAA-2010-4421, 5th AIAA Flow Control Conference, Chicago, IL, 28 Jun - 1 Jul 2010.

[17] B. P. E. Dano, G.-C. Zha, and M. Castillo, "Experimental Study of Co-Flow Jet Airfoil Performance Enhancement Using Micro Discreet Jets." AIAA Paper 2011-0941, 49th AIAA Aerospace Sciences Meeting, Orlando, FL, 4-7 January 2011.

[18] B. Dano, A. Lefebvre and G-C. Zha, "Flow mixing mechanism of a discrete co-flow jet airfoil," 41st AIAA Fluid Dynamics Conference and Exhibit 27 - 30 June 2011, Honolulu, Hawaii.

[19] G.-C. Zha, "Targeting Flow Non-Linearity of Fluid-Structural Interactions Using Detached Ed dy Simulation of Turbulence." Progress Repost to AFOSR, Grant FA9550-06-1-0198, Aug. 2007.

[20] P. Spalart and S. Allmaras, "A One-equation Turbulence Model for Aerodynamic Flows." AIAA-92-0439, 1992.

[21] Y.-Q. Shen and G.-C. Zha, "Large Eddy Simulation Using a New Set of Sixth Order Schemes for Compressible Viscous Terms ," *Journal of Computational Physics*, vol. 229, pp. 8296–8312, 2010.

[22] G.-C. Zha, Y. Shen, and B. Wang, "An improved low diffusion E-CUSP upwind scheme ," *Journal of Computer & Fluids*, vol. 48, pp. 214–220, 2011.

[23] Y.-Q. Shen and G.-Z. Zha , "Generalized finite compact difference scheme for shock/complex flowfield interaction," *Journal of Computational Physics*, vol. doi:10.1016/j.jcp.2011.01.039, 2011.

[24] Shen, Y.-Q. and Zha, G.-C. and Wang, B.-Y., " Improvement of Stability and Accuracy of Implicit WENO Scheme," *AIAA Journal*, vol. 47, No. 2, pp. 331–344, 2009.

[25] Y.-Q. Shen, G.-C. Zha, and B.-Y. Wang, "Improvement of Stability and Accuracy of Implicit WENO Scheme ," *AIAA Journal*, vol. 47, pp. 331–344, 2009.

[26] Shen, Y.-Q. and Zha, G.-C. and Chen, X.-Y., " High Order Conservative Differencing for Viscous Terms and the Application to Vortex-Induced Vibration Flows," *Journal of Computational Physics*, vol. 228(2), pp. 8283–8300, 2009.

[27] Shen, Y.-Q. and Zha, G.-C. , " Improvement of the WENO Scheme Smoothness Estimator," *International Journal for Numerical Methods in Fluids*, vol. DOI:10.1002/fld.2186, 2009.

[28] G.-C. Zha and E. Bilgen, "Numerical Study of Three-Dimensional Transonic Flows Using Unfactored Upwind-Relaxation Sweeping Algorithm," *Journal of Computational Physics*, vol. 125, pp. 425–433, 1996.

[29] B.-Y. Wang and G.-C. Zha, "A General Sub-Domain Boundary Mapping Procedure For Structured Grid CFD Parallel Computation," *AIAA Journal of Aerospace Computing, Information, and Communication*, vol. 5, No.11, pp. 2084–2091, 2008.

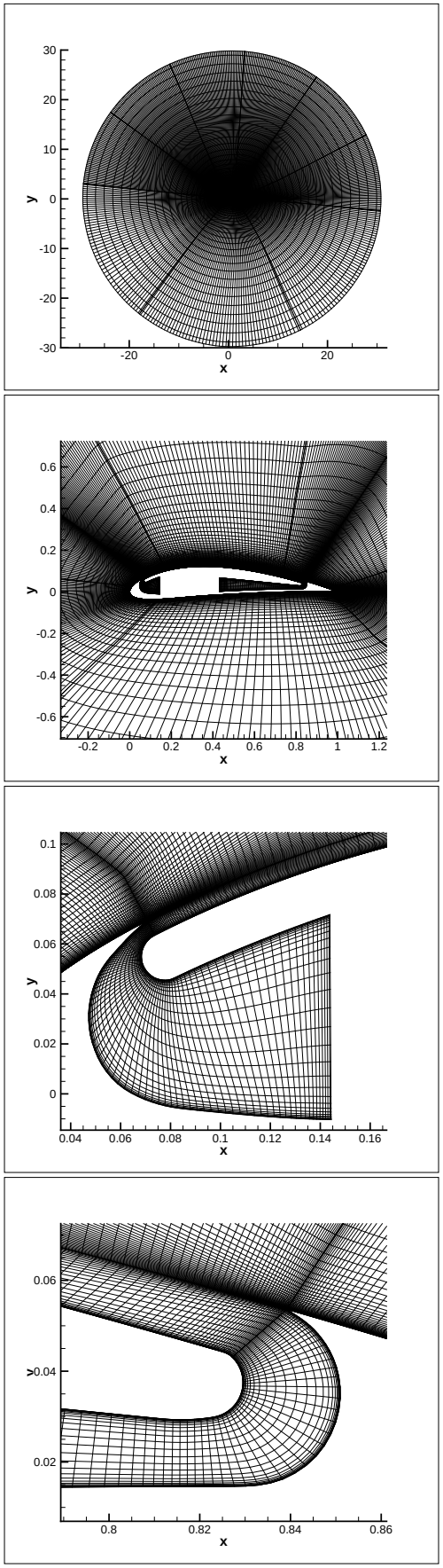

Figure 7: CFJ6415 2D O-mesh topology with detailed view of injection and suction cavity

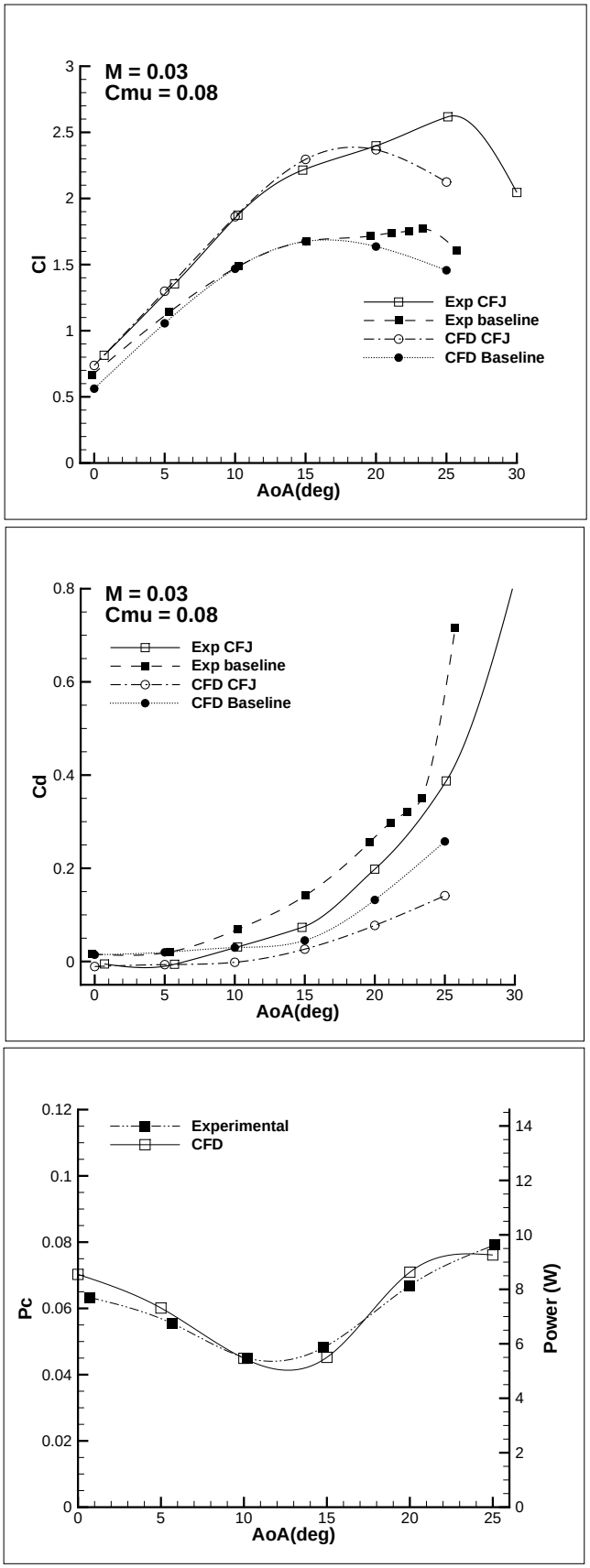

Figure 8: Lift, drag and power coefficient comparison between experimental data and CFD calculations at M=0.03 and $C_\mu = 0.08$

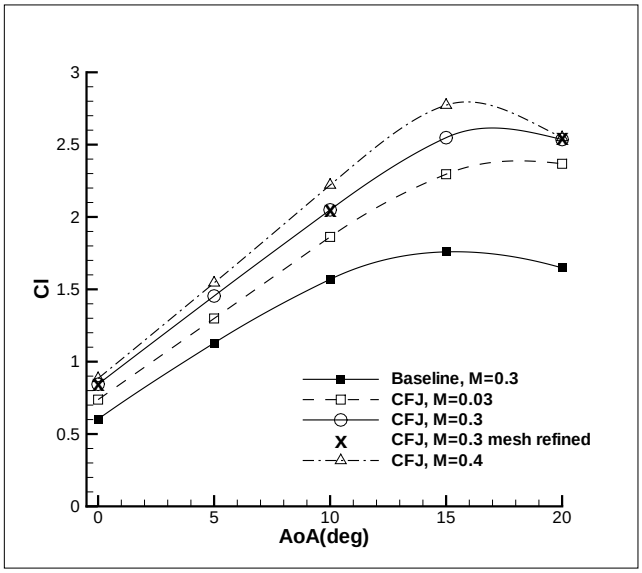

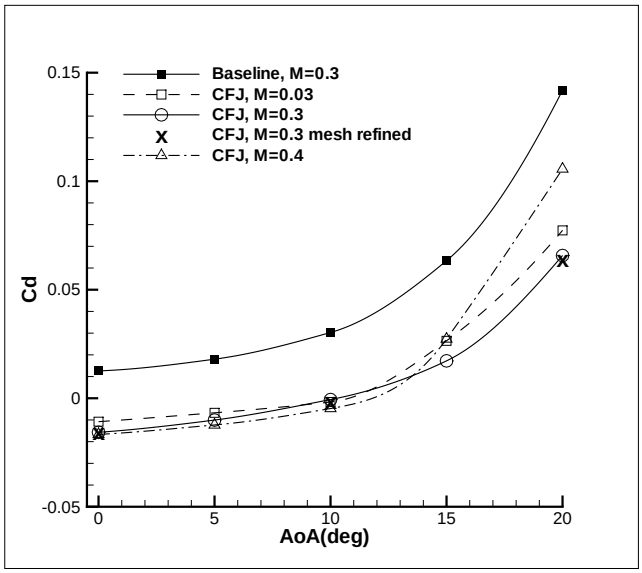

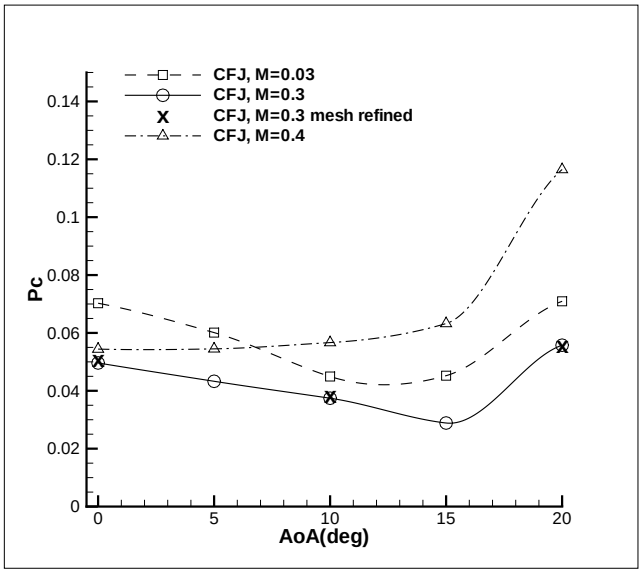

Figure 9: Lift, drag and power comparison from M=0.03 to M=0.4 and $C_\mu = 0.08$

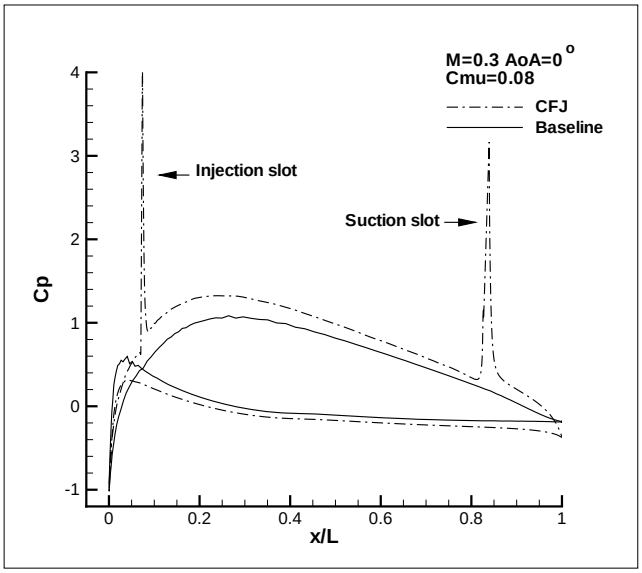

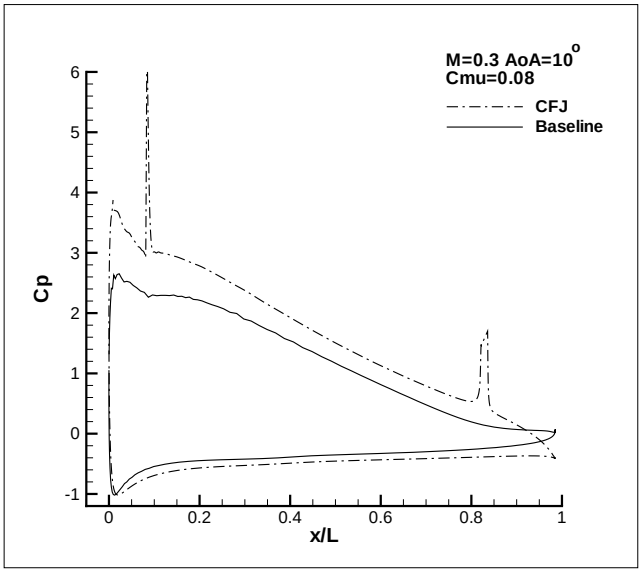

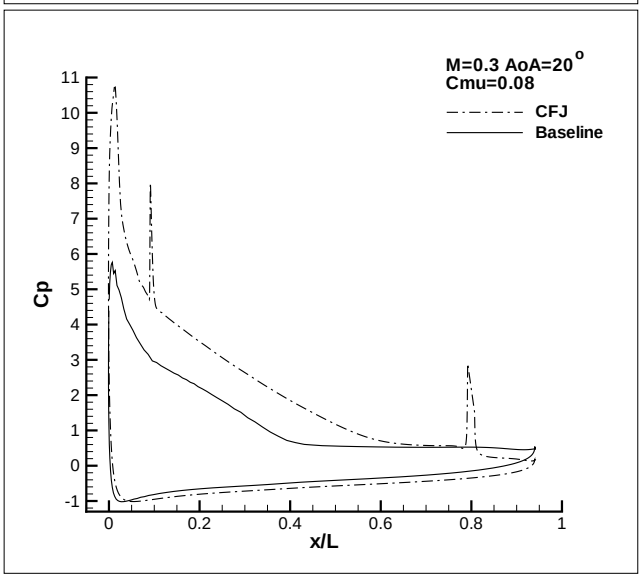

Figure 10: Pressure coefficient comparison between CFJ airfoil and Baseline airfoil at M=0.3 and $C_\mu = 0.08$

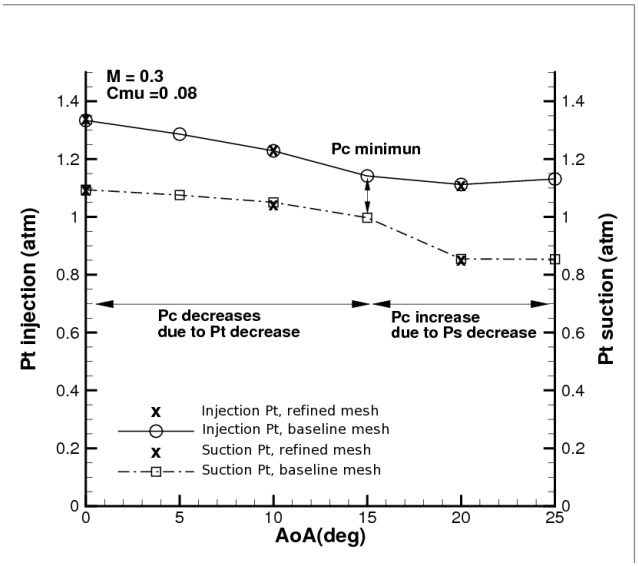

Figure 11: Computed total pressure inside injection and suction cavities at M=0.3 and $C_\mu = 0.08$

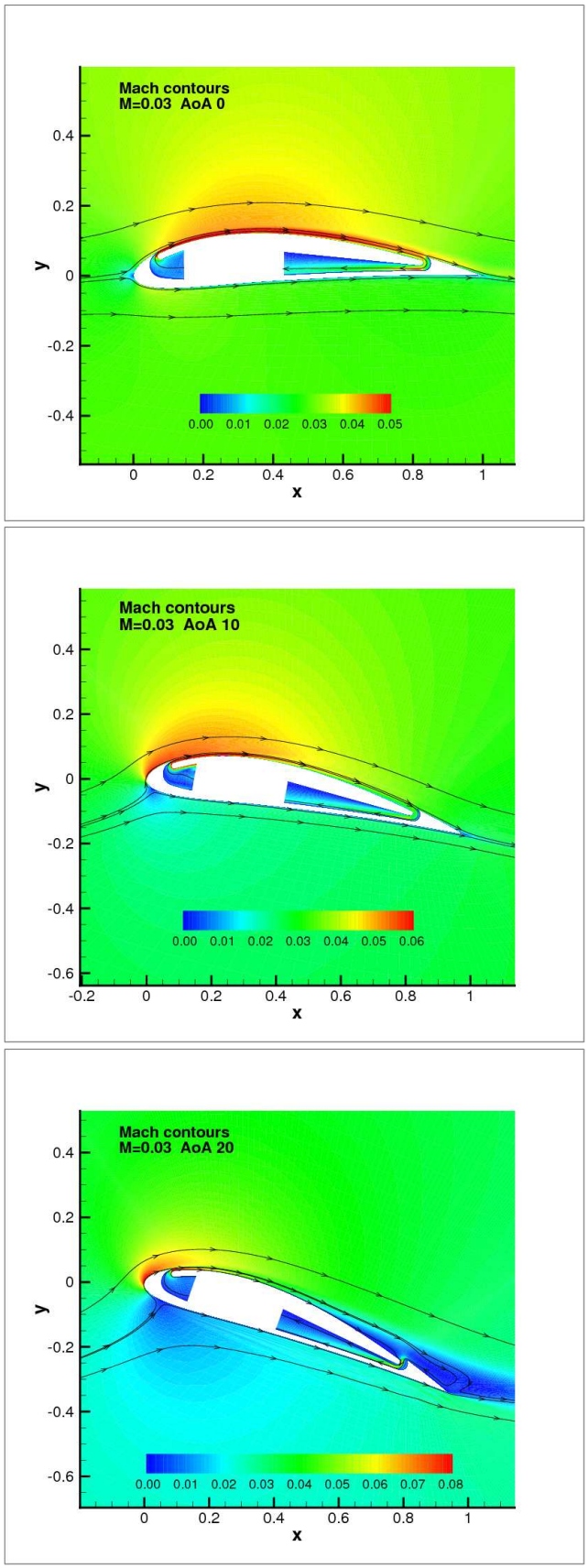

Figure 12: CFJ6415 Mach contour at M=0.03 and $C_\mu = 0.08$ for AoA 0° (top), 10° (middle) and 20° (bottom)

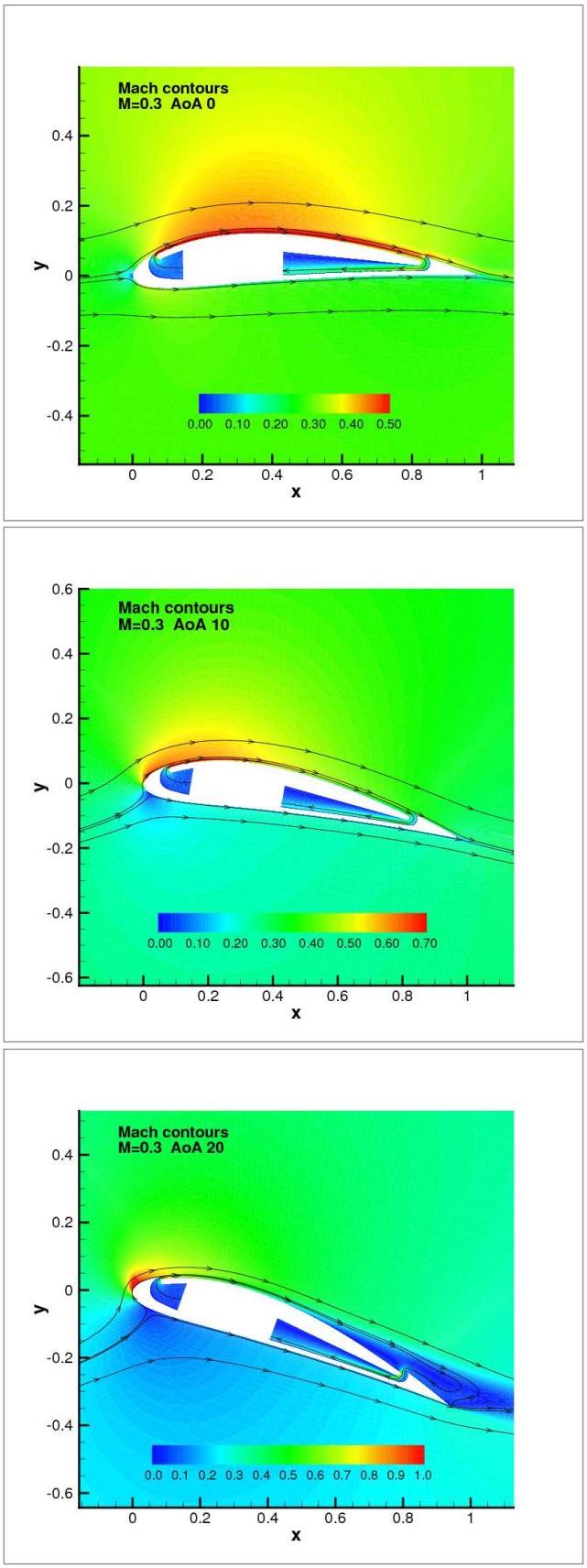

Figure 13: CFJ6415 Mach contour at M=0.3 and $C_\mu = 0.08$ for AoA 0° (top), 10° (middle) and 20° (bottom)

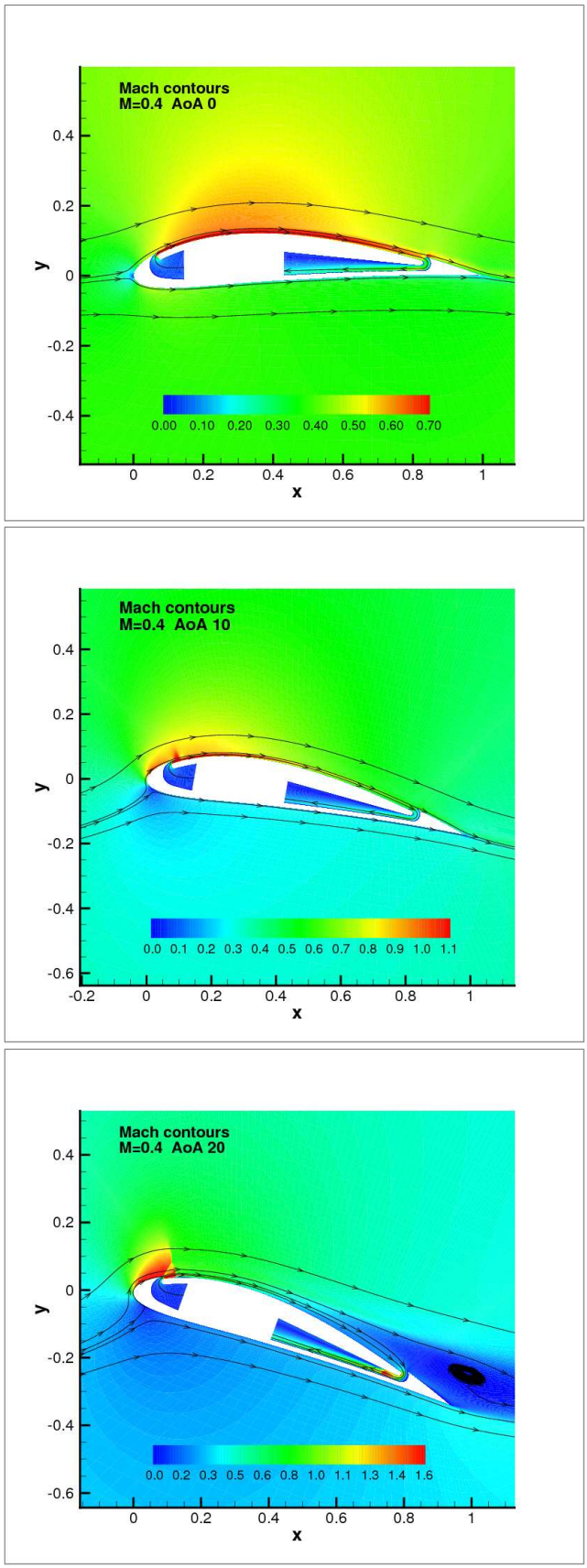

Figure 14: CFJ6415 Mach contour at M=0.4 and $C_\mu = 0.08$ for AoA 0° (top), 10° (middle) and 20° (bottom)

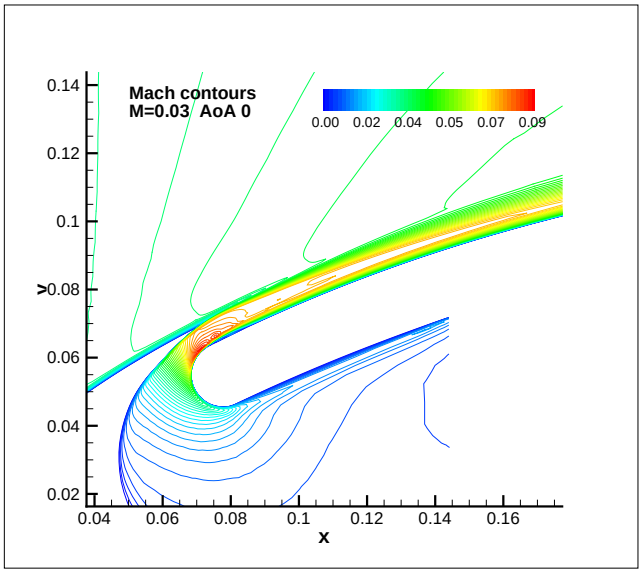

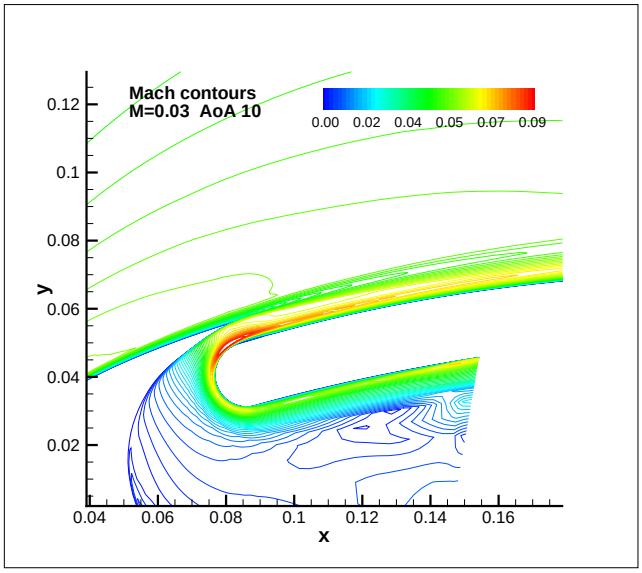

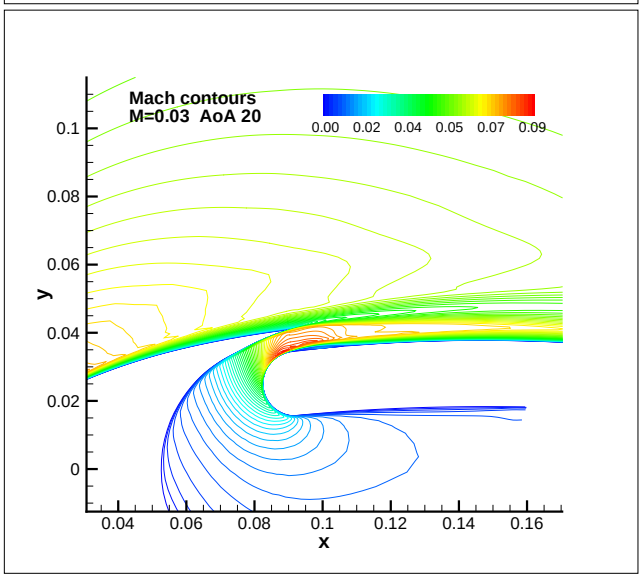

Figure 15: Jet region Mach number line contour at M=0.03 and $C_\mu = 0.08$ for AoA 0° (top), 10° (middle) and 20° (bottom)

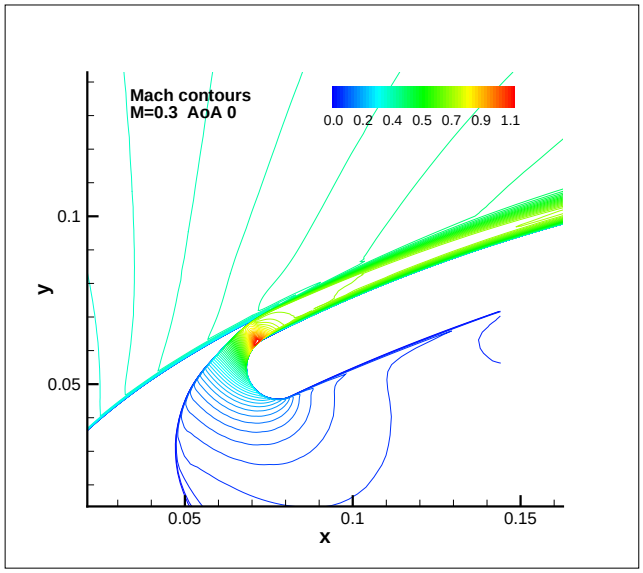

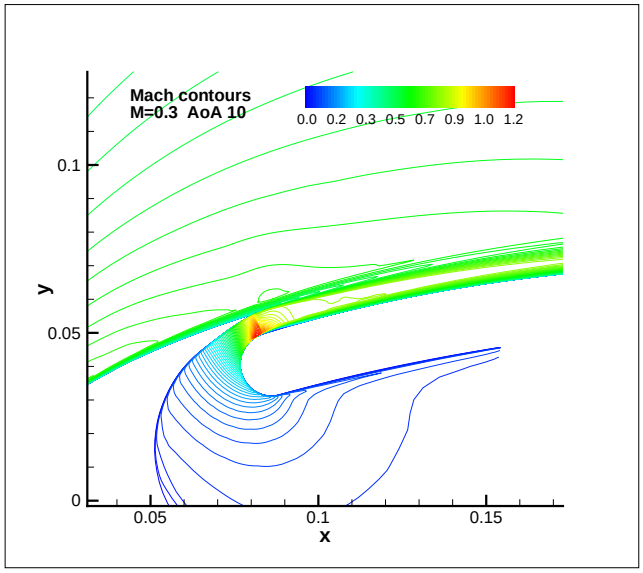

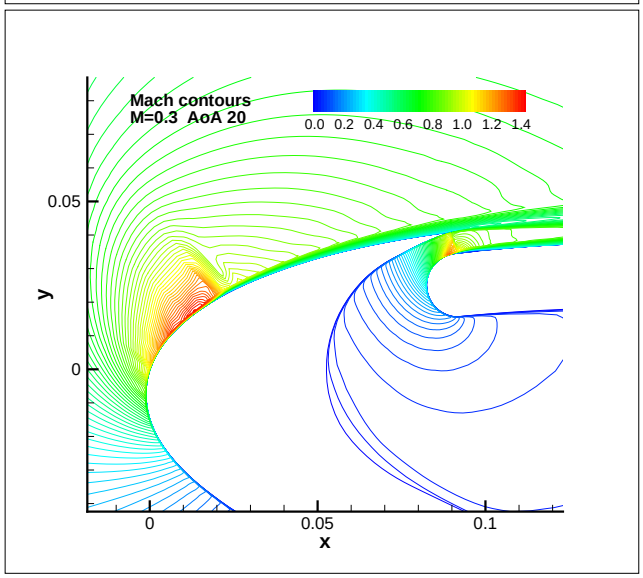

Figure 16: Jet region Mach number line contour at M=0.3 and $C_\mu = 0.08$ for AoA 0° (top), 10° (middle) and 20° (bottom)

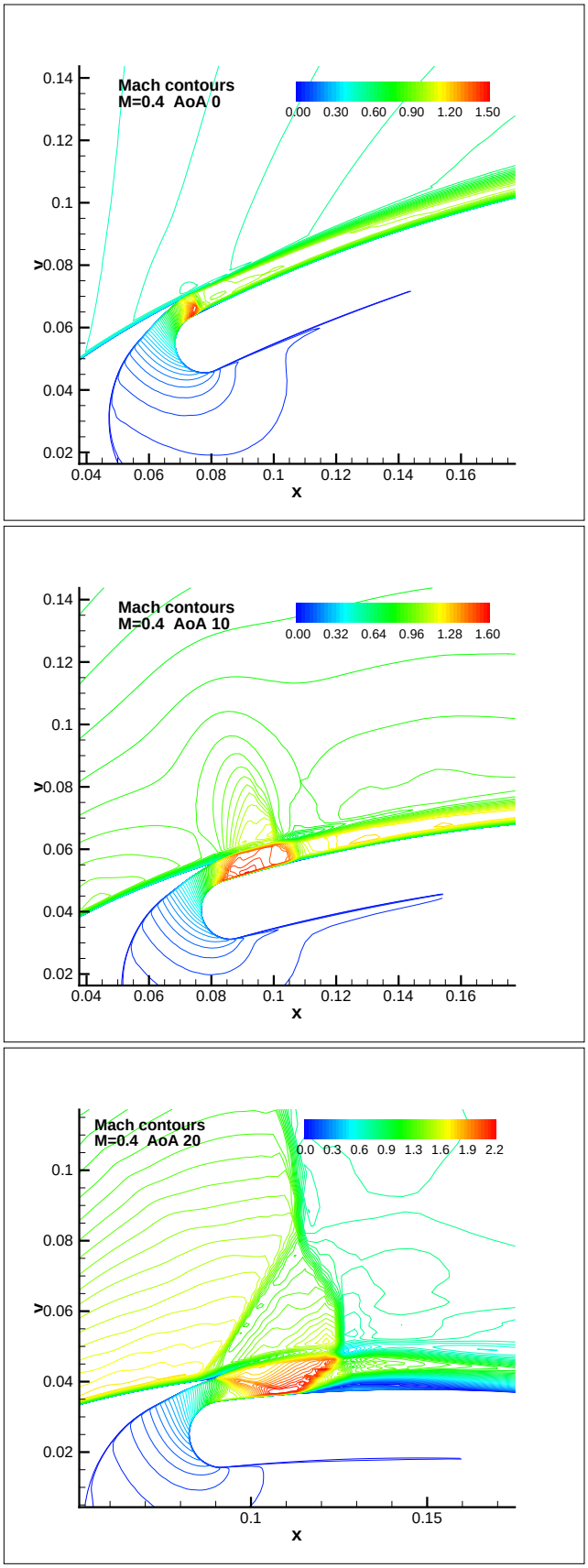

Figure 17: Jet region Mach number line contour at M=0.4 and $C_\mu = 0.08$ for AoA 0° (top), 10° (middle) and 20° (bottom)